

Experimental evidence of long-range correlations and self-similarity in plasma fluctuations*

B. A. Carreras,[†] B. Ph. van Milligen,^{a)} M. A. Pedrosa,^{a)} R. Balbín,^{a)} C. Hidalgo,^{a)}
 D. E. Newman, E. Sánchez,^{a)} R. Bravenec,^{b)} G. McKee,^{c)} I. García-Cortés,^{a)} J. Bleuel,^{d)}
 M. Endler,^{d)} C. Ricardi,^{e)} S. Davies,^{f)} G. F. Matthews,^{f)} E. Martines,^{g)}
 and V. Antoni^{g)}

Oak Ridge National Laboratory, Oak Ridge, Tennessee 37831-8070

(Received 16 November 1998; accepted 12 January 1999)

To better understand long time transport dynamics, techniques to investigate long-range dependences in plasma fluctuations have been applied to data from several confinement devices including tokamaks, stellarators, and reversed field pinch. The results reveal the self-similar character of the edge plasma fluctuations. This implies that the tail of the autocorrelation function decays as a power law and suggests that there is a superdiffusive component of the anomalous transport. Rescaled fluctuation and turbulent flux spectra from different devices also show a strong similarity. For a range of parameters corresponding to the tokamak ohmic regime and equivalent power for other devices, the spectral decay index may show a universal character.

[S1070-664X(99)92405-9]

I. INTRODUCTION

One of the characteristic properties of self-organized criticality systems¹ is that these systems relax through transport events of all sizes (transport by avalanches). This transport mechanism translates to long-range time and space correlations for fluctuating quantities. In such systems, both the correlation functions and the probability distribution function (PDF) of fluxes have algebraic tails. Because self-organized criticality dynamics can explain some of the properties of transport in magnetically confined plasmas,^{2,3} techniques for quantifying the asymptotic behavior of the correlation functions and PDFs are needed. In this paper, we review some of these techniques and their application to plasma fluctuations. In developing and applying these techniques, we have often used the running sandpile model^{1,3-5} as a guidance.

One feature of the turbulence-induced fluxes at the plasma edge is that they are bursty. A PDF of these fluxes shows a long tail with 10% of the largest flux events being responsible for 50% of the transport.^{6,7} These large flux events correspond to Mandelbrot's Noah effect.⁸ The importance of such events is associated with algebraic tails of the PDF of integrated fluxes. In these algebraic tails, there are events of ever increasing size, occurring ever more rarely but still playing a dominant role in the transport.

In the case of plasma fluctuations, we have to specify what we mean by long-range time and radial correlations.

The standard decorrelation time and radial correlation length are determined by the half-width of the corresponding correlation function. The decorrelation time, τ_c , is basically an eddy turnover time, and at the plasma edge of an ohmic plasma it is of the order of several microseconds. We can expect τ_c to also be of the order of the inverse linear growth rate of the dominant microinstability. The radial correlation length, l_c , is of the order of an eddy size, and at the plasma edge it is about 1 cm. Theoretically, it is expected to be of the order of the ion Larmor radius, ρ_i . At the plasma edge, $\rho_i \cong 0.1$ cm is much smaller than the simple theoretical expectation. However, this discrepancy is not what concerns us in this paper; we want to characterize the long-range dependences in the fluctuation data. A series X_t is said to have long-range dependences if its autocorrelation function, $\rho(X_t, X_{t+\Delta})$, asymptotically decays as an algebraic function for long lags, Δ ; that is, if $\rho(X_t, X_{t+\Delta}) \approx \Delta^{-\beta}$ when $\Delta \rightarrow \infty$. The tail of the autocorrelation function of plasma fluctuations is what we are trying to characterize in this paper for both time and radial scales. The order of these scales are many times the basic τ_c and l_c scales of the turbulence.

The usual way of characterizing long-range dependences is by the Hurst exponent, H .^{8,9} This exponent is simply related to the decay index β of the autocorrelation function, $H = 1 - \beta/2$. For experimental data, it is difficult to directly determine H because noise usually dominates the autocorrelation function at long lags. However, there are alternative techniques such as the rescaled range analysis^{8,10} and the scaled window variance techniques.¹¹⁻¹³ We have applied these techniques to analysis of electrostatic plasma edge fluctuations on a broad range of magnetic configurations. They lead to values of H between 0.62 and 0.75.¹⁴ These results are evidence of the existence of long-range correlations in the plasma edge turbulence in those confinement devices. This is Mandelbrot's Joseph effect.⁸ They also show the self-

*Paper U9I2.3 Bull. Am. Phys. Soc. **43**, 1920 (1998).

[†]Invited speaker.

^{a)}Asociación Euratom-Ciemat, 28040 Madrid, Spain.

^{b)}University of Texas, Austin, TX.

^{c)}University of Wisconsin/General Atomics, San Diego, CA 92186-5608.

^{d)}Max-Planck-Institut für Plasmaphysik, Euratom Association, 85740 Garching, Germany.

^{e)}Dipartimento di Fisica, Università di Milano, Italy.

^{f)}JET Joint Undertaking, Abingdon, Oxon, OX14 3EA, U. K.

^{g)}Consorzio RFX., Padova, Italy.

similar nature of the plasma edge fluctuations. The narrow range of variation of H suggests a universal character of the plasma edge turbulence dynamics.

Additionally, this narrow range of values for H found in different plasma confinement devices is also an indication of the similarity of the low-frequency range of the fluctuation spectra in those experiments. However, the similarity of spectra goes beyond the low-frequency range. Using a rescaling transformation of the spectra, we find clear evidence of the similarity of the plasma edge electrostatic fluctuation spectra over the whole frequency range.¹⁵

Some of the techniques used in the detection of the long-range time dependences can be extended to the detection of cross correlations for long time lags.¹⁶ This extension allows the determination of radial correlations and allows comparisons with the radial correlations expected from avalanche transport. This technique has initially been applied to the multichord beam emission spectroscopy (BES) data from DIII-D.

The existence of long-range time correlations and radial correlations at large time lags is expected from self-organized criticality dynamical behavior, but it is not the unique signature of the dynamics of self-organized criticality. Therefore, we can only state that the results of the analysis presented here are consistent with self-organized criticality dynamics. However, they give us two important facts about the plasma turbulence in magnetically confined plasmas that go beyond the validity of the self-organized criticality concept. First, the electrostatic fluctuations over times longer than an eddy turnover time are not constrained with Gaussian statistics. Second, there is a universal character of the fluctuations, at least in the plasma edge for ohmic and ohmic-like regimes.

Finally, if the long radial correlations in the fluxes exist, they would suggest the possibility of a superdiffusive component in the plasma transport^{17,18} in addition to the usual turbulence-induced diffusion. The existence of such a superdiffusive component has been suggested on the basis of magnetic fluctuation-induced transport.¹⁹ Here, we show that similar results can be obtained in a self-organized criticality model. Therefore, superdiffusivity may result from both magnetically and electrostatically induced plasma transport. Such a superdiffusive component is consistent with the Bohm-type scaling observed in tokamak plasma transport in the low confinement mode. A direct experimental determination of such a superdiffusive component is a future challenging goal.

II. ANALYSIS OF LONG-RANGE TIME CORRELATIONS

Many techniques have been proposed to determine the long-range correlations in a time series. One of the first approaches was the rescaled range method, pioneered by Mandelbrot and Wallis.^{8,9} This was followed by several others, among them the scaled windowed variance method^{10–12} and the dispersional method.^{20,21} Here, we apply these methods to the electrostatic plasma edge fluctuations and discuss the relative merits of each technique with regard to the fluctuation data analysis.

The generic idea behind those methods is the creation of a series by averaging over subsets of original time series.²² Given a time series of length n , $X \equiv \{X_t : t = 1, 2, \dots, n\}$, corresponding to a stationary process, all second-order properties of this time series are given by the autocovariance function $\gamma_\Delta = \text{cov}(X_t, X_{t+\Delta})$, where Δ is the time lag. An alternative representation of the second-order properties of this series can be constructed through averaging the original time series over nonoverlapping blocks. That is, for each $m = 1, 2, \dots, n$, we construct a new time series, $X^{(m)} \equiv \{X_u^{(m)} : u = 1, 2, \dots, n/m\}$, with n/m elements by first generating a partition of the original one in n/m nonoverlapping blocks of m elements. Each element of the new series is then obtained by averaging the m elements in each of the blocks. That is, $X_u^{(m)} = (X_{um-m+1} + \dots + X_{um})/m$. For each of the new $X^{(m)}$ series, we can define its variance $V^{(m)}$. It has been observed that the ratio of the logarithm of $\sqrt{V^{(m)}/V^{(1)}}$ to the logarithm of the scale m is $1 - D$, where D is the fractal dimension of the series. D is also related to the Hurst exponent,^{8,9} $H = 2 - D$, which, as discussed later on in this section, is also a measure of the decay exponent of the autocorrelation tail.

The variance of the subseries $X^{(m)}, V^{(m)}$, can also be directly related to the autocovariance function. By direct calculation of $V^{(m)}$, we obtain

$$V^{(m)} = \frac{V^{(1)}}{m} + \frac{2}{m^2} \sum_{s=1}^m \sum_{\Delta=1}^{s-1} \gamma_\Delta. \quad (1)$$

In this relation, the short- and long-range contributions are explicitly separated. For a random variable, X , the first term in the right-hand side (rhs) of Eq. (1) dominates, and in the limit of large m , we obtain the Gaussian statistics result; that is, the standard deviation decreases as 1 over the square root of the number of samples considered. However, for processes with long-range time dependence, the second term may diverge in the large m limit. In this situation, X does not verify the conditions of the central limit theorem, and $V^{(m)}$ does not scale as m^{-1} . Equation (1) can also be used to calculate the autocovariance function of the original series in terms of the variance of the successive averaged subseries. Inverting Eq. (1), we obtain

$$\gamma_\Delta = \frac{1}{2} \partial^2 [\Delta^2 V^{(\Delta)}]. \quad (2)$$

Here, the operator ∂^2 is the second-order central derivative operator in finite differences, that is, $\partial^2(f_i) = f_{i+1} + f_{i-1} - 2f_i$. Equation (2) shows that the information in the variance for all time series $X^{(m)}$ resulting from averaging the original sequence is equivalent to the information contained in the autocovariance function for the original series, X . Therefore, for an infinite series, $V^{(m)}$ provides an alternative equivalent description of the second-order properties of the original series. The advantage of using $V^{(m)}$ to determine the asymptotic behavior of the autocorrelation function instead of using γ_m directly is that the latter is a second derivative of the former. Therefore, small oscillations in $V^{(m)}$ are amplified in γ_m . For noisy signals, it is practically impossible to extract the scaling behavior from γ_m , but in many cases it is possible, even straightforward, from $V^{(m)}$.

When there are long-range correlations in the series X , the covariance function has an algebraic tail, that is $\gamma_\Delta \propto \Delta^{-\beta}$ for large time lag Δ , where $\beta = 2 - 2H$. Therefore, Eq. (2) is the basis for one of the methods of determining H , the so-called dispersive method. In the case of an algebraic tail in the covariance function, we have $V^{(m)} \propto m^{2H-2}$. Because of the smoother dependence of $V^{(m)}$ on m , it is considerably easier to determine the exponent H from $V^{(m)}$ rather than directly from the covariance function.

An alternative method of calculating H is the scaled window variance method. With this method, instead of considering directly the series X , we first construct the associated series of the Brownian motion, that is, the original series integrated in time. For the Brownian motion series and for each $m = 1, 2, \dots, n$, a partition of the series is generated as previously described. We then calculate the standard deviation, $\sigma_m^{(i)}$, within each of the n/m blocks of m elements of this series, and after we average $\sigma_m^{(i)}$ over the n/m blocks, $\sigma_m = (m/n) \sum_{i=1}^{n/m} \sigma_m^{(i)}$.

It can be shown that in case of a series X with a covariance that has an algebraic tail, the function σ_m scales as $\sigma_m \propto m^H$, where H is again the Hurst exponent. This is the scaled window variance method of calculating H .

A third technique, which historically was the first, for evaluating H is the rescaled range statistics proposed by Mandelbrot and Wallis⁸ and is based on the previous hydrological analysis of Hurst.⁹ The R/S ratio is defined as the ratio of the maximal range of the integrated signal normalized to the standard deviation, which we denote here by $S(n)$ to keep the traditional notation. It is defined as

$$\frac{R(n)}{S(n)} = \frac{\max(0, W_1, W_2, \dots, W_n) - \min(0, W_1, W_2, \dots, W_n)}{\sqrt{S^2(n)}} \quad (3)$$

Here $W_k = X_1 + X_2 + \dots + X_k - k\bar{X}(n)$, where $\bar{X}(n)$ is the mean. For phenomena characterized by long-range time dependence, the expected value of R/S scales as $E[R(n)/S(n)] \xrightarrow{n \rightarrow \infty} \lambda n^H$. Here, $E[x]$ is the expected value of the variable x .

For a given series, these three methods should give, in principle, the same value of H . When $1 > H > 0.5$, there are long-range time correlations (persistence) and when $0.5 > H > 0$, the series has long-range anticorrelations (antipersistence). For time series with no time correlations (i.e., random), $H = 0.5$.

In Ref. 23, we analyzed plasma edge Langmuir probe measurements from three stellarators, TJ-IU,²⁴ Wendelstein 7 Advanced Stellarator (W7-AS),²⁵ and the Advanced Toroidal Facility (ATF),²⁶ in the electron cyclotron heating (ECH) regime; two tokamaks, TJ-I,²⁷ and the Joint European Torus (JET),²⁸ in the ohmic heated regime; and one reversed field pinch, the Reversed-Field Experiment (RFX).²⁹ The main result of our analysis is that, for all data sets, the Hurst parameter is constant and well above 0.5 over a self-similarity range much longer than the turbulent autocorrelation time. This result is a clear indication of the existence of long-range time dependencies in the fluctuation dynamics.

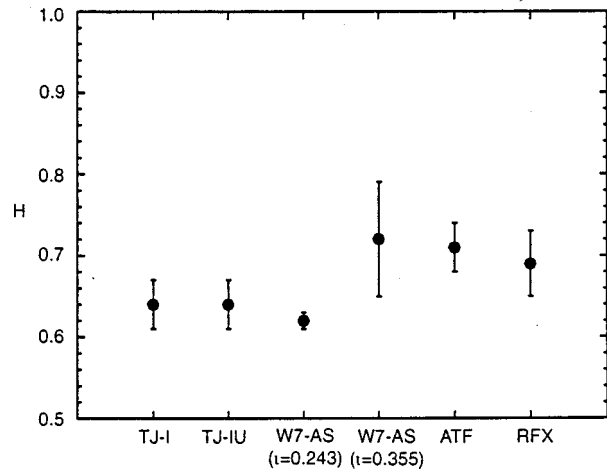


FIG. 1. Hurst exponent for plasma edge Langmuir probe measurements from three stellarators, TJ-IU (Ref. 24), W7-AS (Ref. 25), and ATF (Ref. 26), in the ECH heated regime; and one tokamak, TJ-I (Ref. 27), in the ohmic heated regime and on RFP and RFX (Ref. 29).

Within the plasma edge, the averaged Hurst parameter varies between 0.62 and 0.72, as shown in Fig. 1. This range of variation is relatively small, given the diversity of plasma confinement devices considered. However, for the electrostatic plasma edge fluctuations in the Thorello device, the Hurst exponent is about 0.5. Interestingly, this device has only a toroidal field, therefore, there is no plasma confinement in such a device.

When simultaneous measurements of density and potential fluctuations at two poloidal positions exist, it is possible to reconstruct the local turbulent flux. The time records of the turbulent flux show long-range correlations that are similar to the correlations observed in the fluctuations. For example, in Fig. 2, we have plotted the Hurst exponent for both the ion saturation current and the local turbulent flux as measured in the W7-AS device and for a rotational transform at the edge of $\iota = 0.254$.

The rescaled range method has been shown to be robust for time series generated by fractional Gaussian noise and plasma fluctuation data. However, for the latter, there is a potential problem with the interpretation that was not completely resolved. The problem is a possible alternative expla-

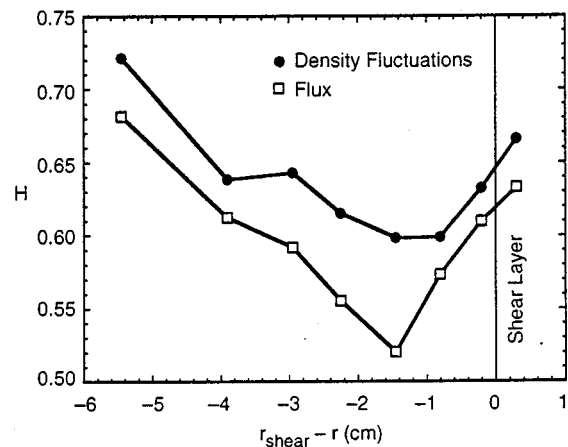


FIG. 2. Hurst exponent for both the ion saturation current and the local turbulent flux as measured in the W7-AS device, and for a rotational transform at the edge of $\iota = 0.254$.

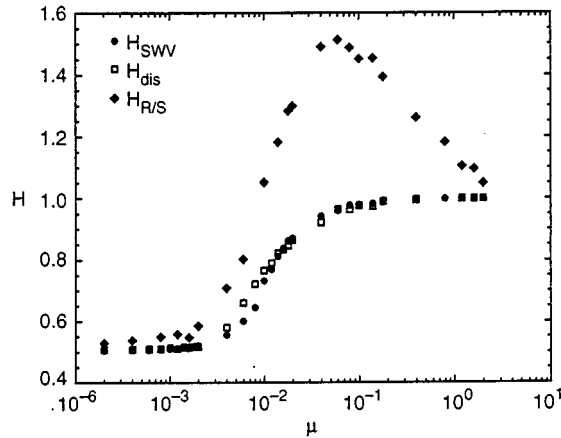


FIG. 3. Hurst exponent determined with the scaled window variance, dispersive, and rescaled range methods as a function of μ , the square root of the ratio of the variance of a sinusoidal signal to the variance of the added random noise.

nation to the existence of long-range correlations in the plasma turbulence, based on the existence of low-amplitude low-frequency coherent or quasiscoherent modes mixed with larger amplitude Gaussian turbulent fluctuations. In such a situation, Hurst exponents between 0.5 and 1.0 can be obtained without the presence of intrinsic long-range correlations in the plasma turbulence.

To test this possible interpretation, we have evaluated H for several time records created by adding a sinusoidal signal to a random noise. These values of H are plotted in Fig. 3 as a function of μ , where μ is the square root of the ratio of the variance of the sinusoidal signal to the variance of the random noise. For each value of μ , we have used five samples of 50 000 points. The Hurst exponent has been calculated using the methods previously discussed. The rescaled range method produces a resonance effect already discussed in Ref. 23. The scaled window variance method is not affected by this resonance, as is clear from Fig. 3, but when it is modified as suggested by Cannon³⁰ through the introduction of a linear trend connection, it also shows the resonance effect. For the dispersive method, the range of time over which H is constant is shorter than for the scaled window variance method, and the H exponent is more difficult to determine. Therefore, the scaled window variance method seems to be the most effective in reducing the probability of contamination by coherent mode effects. The range of H values from the experiment, $0.62 < H < 0.72$, corresponds to a very narrow range of values of μ , that is, $2.1 \times 10^{-3} < \mu < 4.0 \times 10^{-3}$. To explain all of the experimental results, it would be necessary to always have a quasiscoherent mode present in the plasma with an amplitude within this narrow range. Although this situation is possible in some particular cases, it is highly unlikely to be the explanation for all cases analyzed.

Using these analysis methods, we have obtained results very similar to those previously obtained with only the rescaled range method. As an illustration of the similarity of the results, we have plotted in Fig. 4 the values of H obtained with the scaled window variance method versus the ones

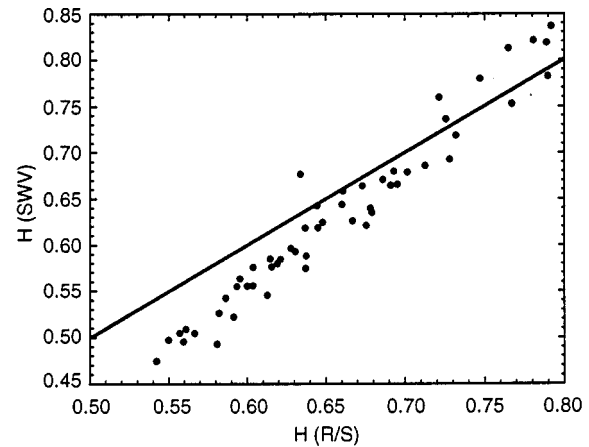


FIG. 4. Values of H obtained with the scaled window variance method versus ones obtained using the rescaled range method for several subseries of the W7-AS data of 1 msec length digitized at 2 MHz.

obtained using the rescaled range. We have used subseries of the W7-AS data of 1 msec length digitized at 2 MHz. Since the series are relatively short, a broader range than usual of H is obtained. This is in accord with observations in Ref. 30 that the rescaled range method has a slight bias towards 0.75. The convergence of results using the different methods gives a further confirmation of the long-range time correlations in the plasma edge fluctuations and their self-similar character.

III. SIMILARITY OF THE FREQUENCY SPECTRA

The small range of values for H in different devices is an indication of the similarity of the fluctuation spectra in the low-frequency range. However, the similarity of spectra goes beyond the low-frequency range. Using a rescaling transformation of the spectra, the similarity of the plasma edge electrostatic fluctuation spectra over the whole frequency range can also be shown. To avoid the distortion of the spectrum caused by the motion of the reference frame, the comparative study of fluctuation spectra in different devices has been done in the proximity of the plasma edge velocity shear layer location, where there is a radial position with $V_{\theta} \approx 0$. For the edge fluctuation measurements considered here, the poloidal velocity is inferred from the plasma velocity of the fluctuations.

In the case of plasma edge fluctuations, the power spectrum, $P(\omega)$, is a function of all plasma parameters. Based on the idea of finite size scaling of the self-organized criticality systems, we had assumed a simple rescaling law,¹⁵ $P(\omega, \dots) = P_0 g(\omega/\omega_0)$, where P_0 and ω_0 are parameters to be determined. The function g , if it exists, reflects the universal character of the underlying dynamical processes.

Frequency spectra for the same plasma edge fluctuations data discussed in the previous section and obtained in TJ-I, TJ-IU, W7-AS, and JET experiments have been rescaled using the TJ-I tokamak as a reference; that is, we take $\omega_0 = 1$ for TJ-I. Figure 5 shows the rescaled frequency spectra of fluctuations for the ion saturation current after the rescaling transformation. The four spectra lie clearly on top of each other. The existence of a unique g function is an indication

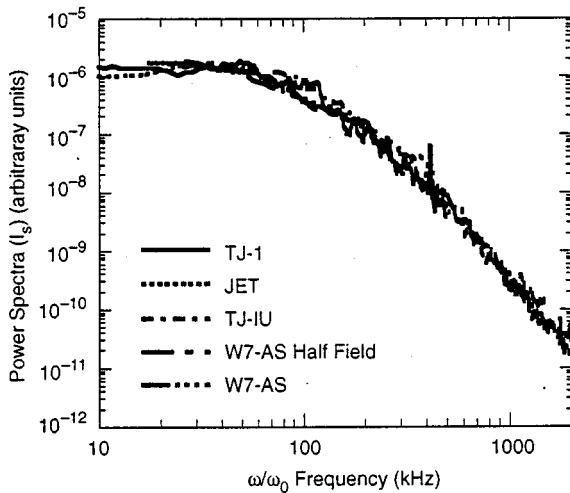


FIG. 5. Rescaled frequency spectra of fluctuations for the ion saturation current in TJ-I ($\omega_0=1$), TJ-IU ($\omega_0=0.33$), W7-AS ($\omega_0=0.286$ and $\omega_0=0.22$), and JET ($\omega_0=0.22$) experiments after the rescaling transformation.

of the universal dynamics of plasma edge turbulence, at least in the parameter regime considered here. Analogous results have been obtained for the power spectrum of the electrostatic potential fluctuations and for the turbulent particle flux. The value of ω_0 varies from device to device, and also with the magnetic field for the same device. The particular value of ω_0 in each case must be given by the dynamics of the plasma turbulence.

It should be noted that while the zero in the velocity is used to remove the Doppler shift effects, this zero usually occurs in a region of large velocity shear. This too could have an effect on the spectrum that is not yet determined.

The generic form of the fluctuation spectra is consistent with decay indexes typical of self-organized criticality systems. If we write the power spectrum in the form $P(\omega) \propto \omega^{-\alpha}$, where α is the decay index, there is a low-frequency region with $\alpha=0$, an intermediate region associated with avalanche overlap with $\alpha=1$ ($1/f$ region), and a high-frequency region with $\alpha>3$. Because the power for these discharges is relatively low, the $1/f$ is expected to be narrow. Analysis of higher power discharges is needed to see if the $1/f$ frequency range broadens with power, as the increase in power will increase the probability of avalanche overlap.⁴

IV. RADIAL CORRELATION OF PLASMA FLUCTUATIONS FOR LONG TIME LAGS

The existence of long-range time correlations and radial correlations at large time lags is expected from self-organized criticality dynamical behavior. The combination of the radial propagation of avalanches and their extended radial structure will induce such correlation. Some of the techniques used in the detection of the long-range time dependences can be extended to the detection of cross correlations for long time lags.¹⁶ So, let us consider two time sequences of length n : the first one, $X \equiv \{X_i; i=1,2,\dots,n\}$, is measured at a radial position r_1 ; and the second one, $Y \equiv \{Y_i; i=$

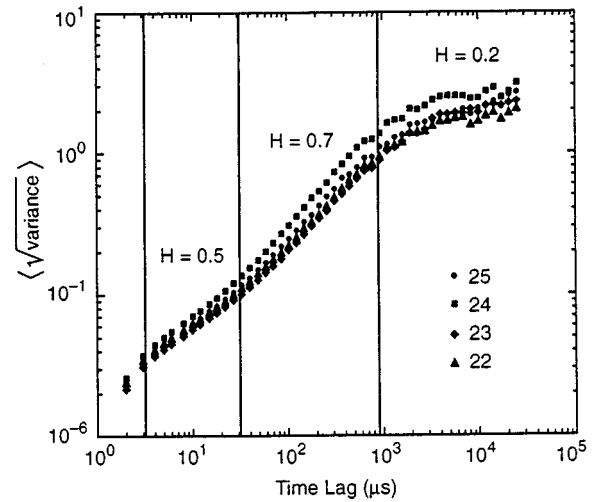


FIG. 6. The result of the scaled window variance analysis for four BES channels.

$=1,2,\dots,n\}$, is measured at a radial position $r_2=r_1+\delta$. For each series, we can calculate the series of partial averages, that is, $X^{(m)} \equiv \{X_u^{(m)}; u=1,2,\dots,n/m\}$ and $Y^{(m)} \equiv \{Y_u^{(m)}; u=1,2,\dots,n/m\}$, where the elements of these series, $X_u^{(m)}$ and $Y_u^{(m)}$, are the average over subblocks. In this case, we arrive at a generalization of Eq. (2),

$$\begin{aligned} 2\gamma_s(m, \delta) &\equiv \gamma^{(1)}(m, \delta) + \gamma^{(1)}(-m, \delta) \\ &= \partial^2[m^2 \gamma^{(m)}(0, \delta)]. \end{aligned} \quad (4)$$

Here, ∂^2 is the second-order finite-difference operator, $\gamma_s(m, \delta)$ is the symmetric component of the cross-covariance, and $\gamma^{(m)}(0, \delta)$ is the cross-covariance of the series $X_u^{(m)}$ and $Y_u^{(m)}$ at zero lag. Equation (4) tells us that calculating the cross-covariance of the partial averages for nonzero time lag is equivalent to calculating the symmetric part of the cross-covariance at finite time lag. As for the autocorrelation, this method is advantageous because by taking the sums, we eliminate some of the high-frequency noise that we are not interested in and that obscures the correlations at long time lags.

This method has been applied to BES data from DIII-D.³¹ This first analysis has been focused on a single shot, 92409. The data were collected during the early phase of a relatively low-power negative-shear discharge. There were 25 channels separated by about 1 cm. For each channel, we have considered a time record of 250 000 points. The digitizing rate was 1 MHz. In the analysis, we have divided each time record in five blocks of 50 000 points, and we have taken the average of all quantities over the five blocks. For the time range analyzed, there is no evidence of sawtooth oscillations or coherent mode activity.

The result of the scaled window variance analysis for all the BES channels shows a common pattern as shown in Fig. 6. In this figure, we have plotted the square root of the variance as a function of time lag for four of the channels analyzed. We can distinguish four scaling regions. Below 4 μsec , the variance is dominated by fluctuations. We will not consider this time range. From about 4 to 30 μsec , the H

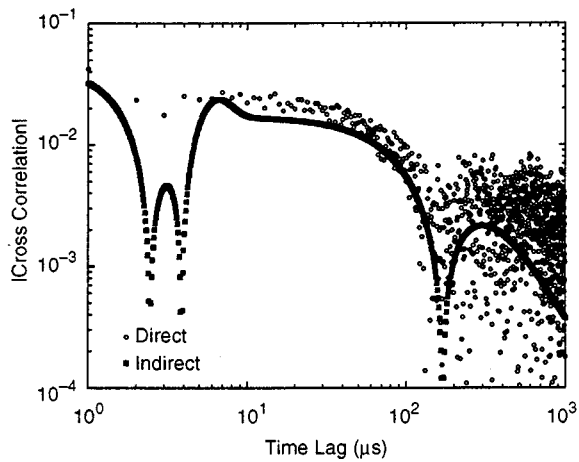


FIG. 7. Absolute value of the symmetric component of the cross-correlation function between two BES channels separated radially about 1 cm. The cross correlation has been calculated in the usual direct way and compared with the method proposed in Ref. 16.

exponent is about 0.5. Between 30 and about 700 μsec , $H \approx 0.7$. Finally, above a few milliseconds, the value of H is around 0.2. The value of H indicates that the second region is dominated by uncorrelated Gaussian noise. This is possibly just the photon noise. The third region is consistent with the presence of long-range time correlations. The last region shows anticorrelation. The results for the last two regions are reminiscent of the rescaled range results for the sandpile flux.¹⁶

Using the method outlined here and described in detail in Ref. 16, we can reconstruct the symmetric component of the cross-correlation function. In Fig. 7, we have plotted the absolute value of the symmetric component of the cross-correlation function between two channels separated radially by about 1 cm. This function has some oscillations at low time lags, shows correlation in the intermediate region where $H \approx 0.7$, and changes to anticorrelation at longer time lags. The structure of the correlation function is quite similar to the one obtained from the correlation of fluxes in a sandpile calculation.¹⁶ In the same figure, we show the result of a direct calculation of the radial cross-correlation using the standard method. We can appreciate the reduction of the level of noise as a result of using the new method of calculation. Similar structure is found for the cross-correlation between other channels. For the region with $H \approx 0.7$, the photon noise is not important; we only need to correct for the effect of the so-called common mode.³² This correction is also small for the range of time lags that we are interested in. The final values of the cross-correlation for the region between 30 and about 700 μsec are plotted in Fig. 8. In this figure, negative values of δ correspond to radial positions outside the position of reference. This figure shows that the radial correlation has its maxima at $\delta \neq 0$ because of the propagation, and its characteristic scale length is of the order of a few centimeters. Here, we have used these data as an example of the method for reconstruction of the correlation. Detailed analysis of other shots is needed to understand the relevance of these results to the self-organized criticality model.

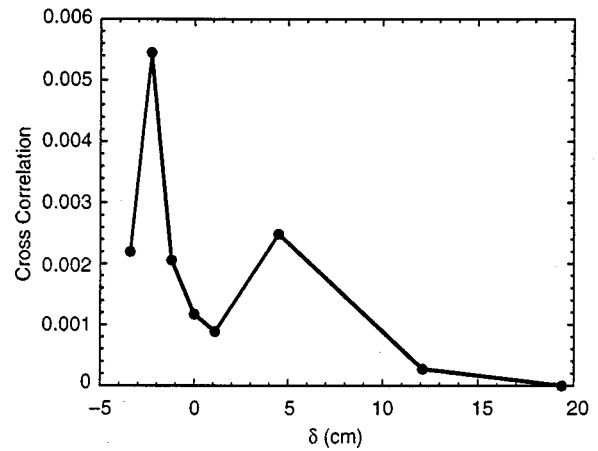


FIG. 8. Radial cross correlation for time lags between 30 μ and about 700 μsec as a function of the radial separation between BES channels. Negative values of δ correspond to radial positions outside the reference position.

V. IMPACT ON TRANSPORT

If long radial and time correlations in the turbulent fluxes exist, they would suggest the possibility of a superdiffusive component in the plasma transport. To test this assumption, we have followed test particles in a running sandpile. The dynamic model for the one-dimensional sandpile closely follows the one in Refs. 1, 4, and 5, and our specific implementation has been discussed in Ref. 3.

We have followed 20 000 particles and calculated the ensemble average of the square of the displacement as a function of time, $\langle r(t)^2 - r(0)^2 \rangle$. Here, the angular brackets indicate ensemble average over the set of test particles. As a function of time, we expect the following dependence, $\langle r(t)^2 - r(0)^2 \rangle = D_0 t^\gamma$. When $\gamma = 1$, the diffusion is called normal, but if $\gamma \neq 1$, the diffusion is anomalous.¹⁸ The calculation is done for sandpiles of varying sizes, from $L = 100$ to 5000. Particles have been followed for distances of the order of a fraction of the sandpile size. For longer excursions, the finite size effects start dominating the dynamics. The results of these calculations give a nearly straight line in log-log plot, indicating that the relation between the square of the displacement and time is essentially a power law. A fit to the data gives values of γ close to 1.5. Because of the finite size of the sandpile, it is difficult to determine the value of γ with enough precision and to narrow its range of variation. The value of γ for different sandpile lengths does not present a dependence on L within error bars.

To understand the dynamical mechanism of the particle transport, we have to look in detail to the properties of the particle orbits. When an avalanche occurs, particles are carried outward. The radial excursion of the particles, flights, depends on the radial extent of the avalanche. In the absence of an avalanche, the particles remain at a fixed radial location. Sometimes particles get buried in the sand, and the time they spend in a given position can be very long. We call those resting periods trapping times. From the information on the particle motion, we can calculate the PDF of both the particle flights and the particle trapping times. The algebraic

tails of these PDFs are consistent with an anomalous diffusion exponent close to 1.5.^{17,18}

Previous calculations of diffusivities in a sandpile were based on the renormalization of a Burgers-like fluid equation.^{2,4} They showed that transport had ballistic character, that is, $\gamma=2$. These calculations corresponded to continuously moving avalanches and did not include the effect of trapping time for the particles. The latter is responsible for the reduction in the value of γ .

In a magnetically confined plasma, the simplest description of the turbulent-induced transport should include at least two components, a diffusive component linked to the basic scales of the fluctuations, l_c and τ_c , and a superdiffusive component linked to the avalanche-induced transport. The latter cannot just be explained by an "anomalous transport coefficient," it requires the use of an anomalous diffusion operator in the transport equations. When the superdiffusive component dominates, the global scaling of confinement time with ρ^* is of the form $\tau \propto (\rho_i^*)^{-2/\gamma}$, with $\gamma > 1$. If γ is close to 2, this scaling is close to Bohm-type transport scaling observed in tokamak plasma during this low confinement mode of operation. The presence of a sheared flow in the plasma may cause the decorrelation of the avalanches,³³ this will suppress the superdiffusive component of the transport. In this case, the global scaling of confinement time with ρ^* is of the form $\tau \propto (\rho_i^*)^{-2}$, that is, it is gyro-Bohm scaling. If the shear in the flow is high enough to suppress the turbulence,³⁴ then both diffusive and superdiffusive components are eliminated and transport is just collisional. This case corresponds to the formation of a transport barrier in the plasma. Therefore, a variety of transport scalings can be expected from this description of the turbulent transport.

VI. CONCLUSIONS

Analysis of the electrostatic edge plasma fluctuations in different confinement devices shows the existence of long-range time correlations. These correlations exist over a time range that goes from the fluctuation decorrelation time to times of the order of confinement time. These results show the non-Gaussian nature of the plasma edge fluctuations.

The similarity of edge plasma fluctuation properties in different devices goes beyond the saturation levels and their radial profile near the edge. A rescaling transformation of the fluctuation power spectra shows the universality of the spectra. These results apply to ion saturation current fluctuations, electrostatic potential fluctuations, and the reconstructed local turbulence flux. Therefore, they strongly suggest a universal mechanism for plasma edge fluctuation dynamics.

The self-organized criticality concept offers a possible framework to explain the universality of the dynamics. To test that hypothesis, it is necessary to identify an avalanche-like mechanism underlying plasma transport. Multichord fluctuation data are needed to detect the long radial correlations induced by the avalanches and their radial propagation. Analysis tools have been developed to carry out this task, and its initial application to DIII-D BES data shows results consistent with such transport mechanisms.

If such a mechanism is confirmed, it offers a way to explain such diverse phenomena as Bohm-scaling of transport in L-mode (low confinement mode) discharges, nondiffusive behavior of perturbative experiments, and resilience of profiles. It also implies that the anomaly in the plasma transport cannot just be explained by an "anomalous transport coefficient," but that it requires the use of an anomalous diffusion operator in the transport equations.

ACKNOWLEDGMENTS

We acknowledge useful discussions with P. H. Diamond and G. M. Zaslavsky. Research was sponsored by the Oak Ridge National Laboratory, managed by Lockheed Martin Energy Research Corp. for the U.S. Department of Energy under Contract No. DE-AC05-96OR22464.

- ¹P. Bak, C. Tang, and K. Wiesenfeld, *Phys. Rev. Lett.* **59**, 381 (1987).
- ²P. H. Diamond and T. S. Hahm, *Phys. Plasmas* **2**, 3640 (1995).
- ³D. E. Newman, B. A. Carreras, P. H. Diamond, and T. S. Hahm, *Phys. Plasmas* **3**, 1858 (1996).
- ⁴T. Hwa and M. Kadar, *Phys. Rev. A* **45**, 7002 (1992).
- ⁵L. P. Kadanoff, S. R. Nagel, L. Wu, and S. M. Zhou, *Phys. Rev. A* **39**, 6524 (1989).
- ⁶E. Sánchez, C. Hidalgo, M. A. Pedrosa, R. Balbín, I. García-Cortés, T. Estrada, and B. van Milligen, "On the statistical properties of plasma fluctuations and turbulent transport in TJ-I tokamak and TJ-IU torsatron," in *Chaos and Plasma Physics 2*, edited by S. Benkadda, F. Doveil, and Y. Elskens (World Scientific, Singapore, 1996).
- ⁷M. Endler, H. Niedermeyer, L. Giannone, E. Holzhauser, A. Rudyj, G. Theimer, N. Tsois, and ASDEX Team, *Nucl. Fusion* **35**, 1307 (1995).
- ⁸B. B. Mandelbrot and J. R. Wallis, *Water Resour. Res.* **4**, 909 (1969).
- ⁹H. E. Hurst, *Trans. Am. Soc. Civ. Eng.* **116**, 770 (1951).
- ¹⁰B. B. Mandelbrot and J. R. Wallis, *Water Resour. Res.* **5**, 967 (1969).
- ¹¹B. B. Mandelbrot, *Phys. Scr.* **32**, 257 (1985).
- ¹²M. J. Cannon, D. B. Percival, D. C. Caccia, G. M. Raymond, and J. B. Basingthwaight, *Physica A* **241**, 606 (1997).
- ¹³J. G. Moreira, J. K. L. di Silva, and S. O. Kamphorst, *J. Phys. A* **27**, 8079 (1994).
- ¹⁴B. A. Carreras, B. van Milligen, M. A. Pedrosa *et al.*, *Phys. Rev. Lett.* **80**, 4438 (1998).
- ¹⁵M. A. Pedrosa, C. Hidalgo, B. A. Carreras *et al.*, "Comparative studies of frequency spectra of the edge plasma fluctuations in toroidal magnetic confinement systems," *Phys. Rev. Lett.* (to be published).
- ¹⁶B. A. Carreras, D. E. Newman, B. P. van Milligen, and C. Hidalgo, *Phys. Plasmas* **6**, 485 (1999).
- ¹⁷M. F. Shlesinger, G. M. Zaslavsky, and J. Klafter, *Nature (London)* **363**, 31 (1993).
- ¹⁸G. M. Zaslavsky, in *Levy Flights and Related Topics in Physics*, edited by M. F. Shlesinger, G. M. Zaslavsky, and U. Frisch (Springer, Berlin, 1995), p. 216.
- ¹⁹G. M. Zaslavsky, D. Stevens, and H. Weitzner, *Phys. Rev. E* **48**, 1683 (1993).
- ²⁰J. B. Basingthwaight and G. M. Raymond, *Ann. Biomed. Eng.* **23**, 491 (1995).
- ²¹J. B. Basingthwaight, L. S. Liebovitch, and B. J. West, *Fractal Physiology* (Oxford U. P., New York, 1994).
- ²²D. R. Cox, in *Statistics: an Appraisal*, edited by H. A. David and H. T. David (Iowa State Univ., Ames, IA, 1984), p. 55.
- ²³B. A. Carreras, B. van Milligen, M. A. Pedrosa *et al.*, *Phys. Plasmas* **5**, 3632 (1998).
- ²⁴C. Hidalgo, M. A. Pedrosa, B. van Milligen *et al.*, in *Fusion Energy 1996* (International Atomic Energy Agency Vienna, 1997), Vol. 1, p. 617.
- ²⁵J. Bleuel, G. Theimer, M. Endler, L. Giannone, H. Niedermeyer, ASDEX Team, and W7-AS Team, in *Controlled Fusion and Plasma Physics* (European Physical Society, Petit-Lancy, 1996) Vol. 20C, p. 727.

- ²⁶C. Hidalgo, J. H. Harris, T. Uckan *et al.*, Nucl. Fusion **13**, 1471 (1991).
- ²⁷I. Garcia-Cortes, M. A. Pedrosa, C. Hidalgo *et al.*, Phys. Fluids B **4**, 4007 (1992).
- ²⁸I. Garcia-Cortes, M. Endler, A. Loarte *et al.*, in *Controlled Fusion and Plasma Physics* (European Physical Society, Petit-Lancy, 1997), Vol. 21A, Part 1, p. 109.
- ²⁹V. Antoni, R. Cavazzana, D. Desideri, E. Martinez, G. Serianni, and L. Tramontin, Phys. Rev. Lett. **80**, 4185 (1998).
- ³⁰H. E. Schepers, J. H. G. M. van Beek, and J. B. Bassingthwaite, IEEE Eng. Med. Biol. Mag. , p. 57 (1992).
- ³¹G. McKee, R. Ashley, R. Durst *et al.*, Rev. Sci. Instrum. **70**, 913 (1999).
- ³²R. D. Durst, R. J. Fonck, G. Cosby, H. Evensen, and S. F. Paul, Rev. Sci. Instrum. **63**, 4907 (1992).
- ³³D. E. Newman, B. A. Carreras, and P. H. Diamond, Phys. Lett. A **218**, 58 (1996).
- ³⁴H. Biglari, P. H. Diamond, and P. W. Terry, Phys. Fluids B **2**, 1 (1990).